Real-Time Multiobjective Optimization in Solar Membrane Distillation Processes

María M. Lozano[1], Juan D. Gil[1], Lidia Roca[2], Manuel Berenguel[1], Manuel Pérez[1], Robin De Keyser[3]

[1]Centro Mixto Ciesol, ceiA3, Universidad de Almería, Almería (Spain)
[2]CIEMAT-Plataforma Solar de Almería, Tabernas (Spain)
[3]DySC research group on Dynamical Systems and Control, Ghent University, Ghent (Belgium)

Abstract

Solar Membrane Distillation (SMD) technology is a promising separation method that uses low-grade solar energy as power source. Despite this technology has not been industrially implemented yet, it is in an advanced phase of maturity so that current research works are mainly focused on the development of suitable operating strategies to improve the Membrane Distillation (MD) modules performance. The intermittent and unpredictable behavior of solar energy as well as the hybrid nature of SMD plants make the development of real-time operating strategies essential. Accordingly, this paper proposes a real-time multiobjective optimization method based on the combination of a state machine and a Nonlinear Model Predictive Control (NMPC) technique for the maximization of the distillate production and the thermal efficiency of the plant, two of the major impediments preventing the commercialization of SMD facilities. Simulation results and a comparison with a manual operating strategy are provided to evidence the benefits achieved with the proposed technique.

Keywords: Solar desalination, Process control, Dynamic simulation, Solar thermal energy, Thermal storage.

1. Introduction

Water demand is increasing steadily due to the growth of the population and the associated socio-economic development of industrial and agricultural activities. In addition, climate change and contamination are aggravating the water problem worldwide so that, some studies report that around 5.7 billion people (around 60 % of the world population) can suffer from water scarcity in 2050 (WWAP, 2018). Taking into account this panorama, desalination methods are getting more and more attention as a way to enhance water supply options in arid or semi-arid areas. However, although desalination stands out as one of the most effective solutions, irresponsible and intensive use of this technology can cause severe environmental problems due to the high energy consumption of current desalination technologies. This problem is even more significant if one considers that only around 1 % of total desalination facilities currently in operation are powered with renewable energy (Ghaffour et al., 2014). Therefore, it is necessary to improve the combination between conventional desalination methods and renewable energies and to explore alternative methods that present better characteristics to be combined with these renewable sources.

In the line of the search for substitute desalination methods, one of the main techniques that is gaining interest in recent decades is the MD technology. MD is a thermally driven separation technique that requires a low operating temperature (between 60-85 ºC). This fact makes the case for combining MD processes with low-grade solar energy, forming sustainable plants that reduce the carbon footprint (Zaragoza et al. 2014). Moreover, the simplicity of the process and its tolerance to both, small-scale decentralized use and intermittent operation, make MD technology one of the most appropriate methods to develop stand-alone desalination plants to be implemented in isolated areas with small-medium water needs and good availability of solar irradiance, as island regions. In fact, this is one of the most favorable applications of MD technology since other desalination techniques significantly increase costs at downscale (Guillén-Burrieza et al. 2015) and normally require on-grid power. Nevertheless, to fully commercialize MD technology, both the design of the modules and the operating strategies must be improved to increase the thermal efficiency and distillate production of MD modules, which are the two of the main drawbacks so far.

Selection and/or peer review under responsibility of Scientific Committee
doi:10.18086/eurosun.2020.03.02 Available at http://proceedings.ises.org

Since the emergence of MD technology in 1963, research efforts have been focused on the search of new membranes and designs of MD modules. These investigations have caused a significant progress in terms of thermal energy as MD modules have gone from an initial thermal consumption of 810 kWh/m^3 (Guillén-Burrieza et al. 2011) to current consumptions of around 49 kWh/m^3 (Andrés-Mañas et al. 2020). That is why MD technology is in a new phase of development in which other research addressing the optimal operation of MD modules, especially when they are coupled with solar energy, are arising (Gil et al. 2020). From the point of view of the operation, the main difficulties presented in these plants appear as a result of their hybrid nature. SMD plants include solar fields and thermal storage devices requiring proper management techniques in real-time according to the thermal storage state, the level of irradiance and operating necessities (i.e., water needs); which is difficult and laborious to perform manually. As a consequence, not long ago, the interest in the application of control and real-time optimization techniques in these kinds of plants has grown (Thomas et al., 2017). For example, in Refs. (Chang et al., 2010; Porrazo et al., 2013) control methods based on ON/OFF controllers or Proportional, Integral and Derivative (PID) controllers aimed at temperature regulation were proposed. These kinds of methods provide adequate strategies to improve the dispatchability of SMD plants, dealing with their hybrid nature and allowing the operators to maintain a desired operating temperature in the MD module. However, they do not consider improving the thermal efficiency and the distillate production of the MD module, the two main metrics used to evaluate its performance. More recently, advanced control strategies based on the Model Predictive Control (MPC) technique have been proposed which are tasked with improving the aforementioned metrics separately (Gil et al., 2018a; Bendevis et al., 2020; Guo et al., 2020). The problem is that to increase the distillate production and thermal efficiency converse operating conditions are required in the feed flow rate of the MD module. Thus, the works referenced above only consider mono-objective optimization problems responsible for improving only one of the metrics in real-time. To the authors' knowledge, there are no works in the literature addressing this multiobjective optimization problem in real-time; what can be fundamental to the proper industrialization of the MD technology.

Based on the above issues, this paper proposes a real-time multiobjective optimization method to improve in real-time both the distillate production and the thermal efficiency. The developed algorithm is composed by two main parts. First, following the ideas presented in our previous work (Gil et al., 2018a), a state machine tasked with selecting the adequate operating mode of the facility is used to deal with the hybrid nature of the plant. Second, an NMPC technique that calculates optimal control actions in real-time according to the operating mode and operating conditions is used to improve the desired objectives. Several simulation tests using a validated model of a real pilot plant located at Plataforma Solar de Almería (PSA) have been carried out from which the benefits of the designed control architecture are demonstrated.

2. System description

In this work, a real pilot plant located at PSA (www.psa.es) has been used as reference to perform the simulation analysis. The schematic diagram of the facility is presented in Fig. 1.

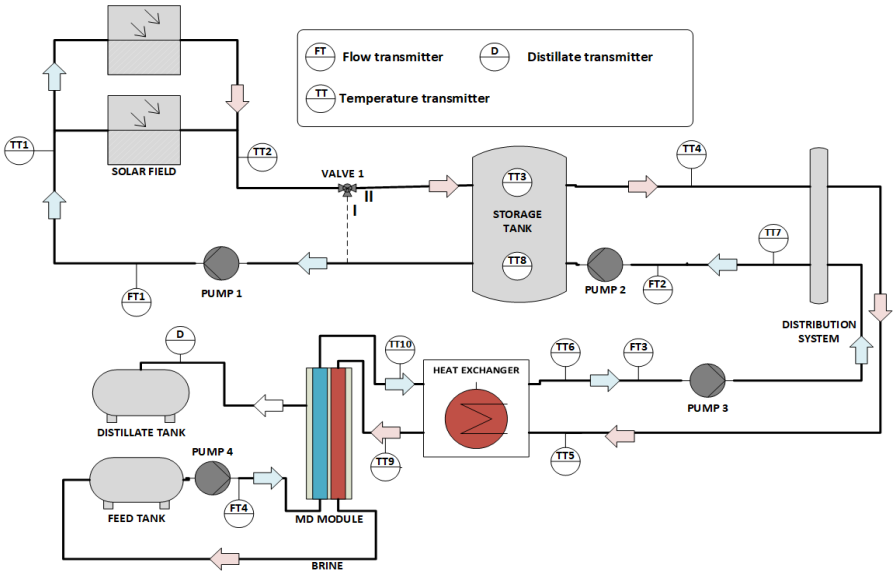

Fig. 1: Schematic diagram of the SMD plant at PSA.

In this facility, the thermal power demanded by the MD unit is provided through a solar thermal field composed of flat-plate collectors, with a total surface area of 22.8 m^2 and a nominal capacity of 7 kW_{th}.This solar field is directly coupled to a thermal storage tank with a capacity of 1500 L. Then, a distribution system is available that connects with a heat exchanger in charge of giving the thermal power to the MD module. The facility is fully monitored and controlled by a Supervisory Control and Data Acquisition (SCADA) system. Tab. 1 of the appendix summarizes the main variables of interest for this work. Please note that a complete description of the plant as well as of the MD module used in this work can be found in (Zaragoza et al. 2014; Gil et al., 2018a) and (Gil et al., 2018b) respectively.

3. System modelling

This section shows an overview of the model of the SMD plant used in both the simulation tests and the predictive control strategy. It should be noted that the whole model was already presented and validated in (Gil et al., 2018a; 2018b).

First, the solar field was modelled by means of a lumped-parameter model given by:

$$A_{sf}\rho c_p \frac{d\mathrm{TT2(t)}}{dt} = \beta \mathrm{I(t)} - \frac{H_1}{L_{eq}}\left(\bar{T}(t) - \mathrm{T}_a(t)\right) - c_p \dot{m}_{eq}(t)\frac{\mathrm{TT2}(t)-\mathrm{TT1}(t)}{L_{eq}}, \quad \text{(eq. 1)}$$

where:

$$L_{eq} = L_a n_{cs}, \quad \text{(eq. 2)}$$

$$\dot{m}_{eq}(t) = \frac{\mathrm{FT1}(t)\rho}{c_1}, \quad \text{(eq. 3)}$$

$$\bar{T}(t) = \frac{\mathrm{TT1}(t)+\mathrm{TT2}(t)}{2}. \quad \text{(eq. 4)}$$

Second, the inlet solar field temperature was characterized by using a static mass balance:

$$\mathrm{TT1}(t) = \mathrm{TT2}(t)\frac{\mathrm{V1}(t)}{100} + \mathrm{TT8}(t)\left(1 - \frac{\mathrm{V1}(t)}{100}\right). \quad \text{(eq. 5)}$$

Third, the storage tank was modelled by using a two-nodes stratified dynamical model which can be described as follows:

$$\frac{d\mathrm{TT3(t)}}{dt} = \frac{1}{\rho V_1}\left(\dot{m}_{sf}(t)\mathrm{TT2}(t) + \dot{m}_{ds}(t)\mathrm{TT8}(t) - \dot{m}_{sf}(t)\mathrm{TT3}(t) - \dot{m}_{ds}(t)\mathrm{TT3}(t) - \frac{H_2(\mathrm{TT3}(t)-\mathrm{T}_a(t))}{c_p}\right), \quad \text{(eq. 6)}$$

$$\frac{d\mathrm{TT8(t)}}{dt} = \frac{1}{\rho V_1}\left(\dot{m}_{sf}(t)\mathrm{TT3}(t) + \dot{m}_{ds}(t)\mathrm{TT7}(t) - \dot{m}_{sf}(t)\mathrm{TT8}(t) - \dot{m}_{ds}(t)\mathrm{TT8}(t) - \frac{H_3(\mathrm{TT8}(t)-\mathrm{T}_a(t))}{c_p}\right), \quad \text{(eq. 7)}$$

where:

$$\dot{m}_{sf}(t) = \frac{\mathrm{FT1}(t)\frac{\mathrm{V1}(t)}{100}\rho}{c_2}, \quad \text{(eq. 8)}$$

$$\dot{m}_{sf}(t) = \frac{\mathrm{FT2}(t)\rho}{c_2}. \quad \text{(eq. 9)}$$

Fourth, the temperatures at both sides of the heat exchanger were adjusted by using a first principles-based static model:

$$\mathrm{TT6}(t) = \mathrm{TT5}(t) - \eta_1\left(\mathrm{TT5}(t) - \mathrm{TT9}(t)\right), \quad \text{(eq. 10)}$$

$$\mathrm{TT10}(t) = \mathrm{TT9}(t) - \eta_2\left(\mathrm{TT5}(t) - \mathrm{TT6}(t)\right), \quad \text{(eq. 11)}$$

where:

$$\eta_1 = \frac{1-e^{\theta}}{1-\frac{\dot{m}_{he}(t)c_p}{\dot{m}_{MD}(t)c_{p,sw}}e^{\theta}}, \quad \text{(eq. 12)}$$

$$\eta_2 = \frac{\dot{m}_{he}(t)c_p}{\dot{m}_{MD}(t)c_{p,sw}}, \quad \text{(eq. 13)}$$

$$\theta = \alpha A_{he}\left(\frac{1}{\dot{m}_{he}(t)c_p} - \frac{1}{\dot{m}_{MD}(t)c_{p,sw}}\right). \quad \text{(eq. 14)}$$

Finally, the MD module was modelled by using an Artificial Neural Network (ANN) model described and validated in (Gil et al., 2018b). This model provides the value of the distillate production (D) and Specific Thermal Energy Consumption (STEC) according to the value of the evaporator channel inlet temperature of the MD module (TT9), the feed water flow rate (FT4), and the operating conditions of the feed water in terms of temperature and salinity. These two lasts are considered constants in this work assuming typical mean values of the Mediterranean Sea, 20 ºC and 35 g/L respectively. Therefore, the ANN model can be generically described as:

$$\mathrm{D}(t) = f(\mathrm{TT9}(t), \mathrm{FT4}(t)), \quad \text{(eq. 15)}$$

$$\mathrm{STEC}(t) = f(\mathrm{TT9}(t), \mathrm{FT4}(t)), \quad \text{(eq. 16)}$$

where $f(\cdot)$ is a function of its arguments given by the ANN model.

It should be remarked that all the constants and parameters involved in the model as well as their units and values are presented in Tab. 2 of the Appendix.

4. Real-time operating strategy

As stated before, one of the main operating problems of MD systems consists of maximizing their distillate production and thermal efficiency in real-time, particularly when they are powered with solar energy. To address this issue, in this paper, a control system is proposed (see Fig. 2) composed of two main parts: i) a state machine and ii) an NMPC controller based on the Nonlinear Extended Prediction Self-Adaptative Control (NEPSAC) algorithm (De Keyser, 2003).

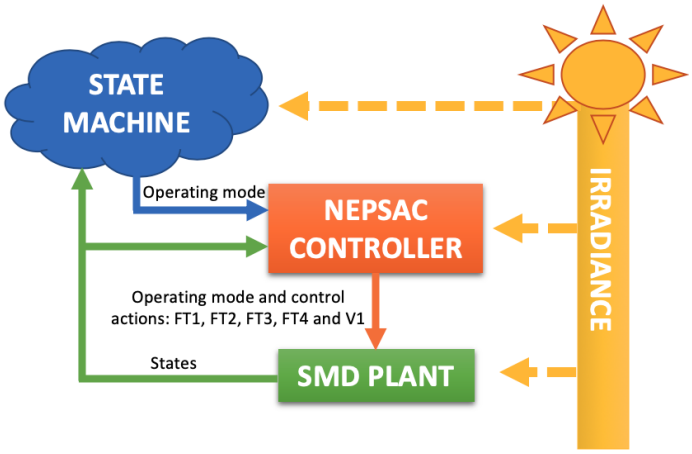

Fig. 2: Schematic diagram of the control system.

On the one hand, the state machine is responsible for dealing with the hybrid nature of the SMD plant. Thus, it receives the states of the real plant and the external operating conditions, i.e. global irradiance, and decides the most appropriate operating mode according to a designed rule-based system. On the other hand, the NEPSAC controller computes the optimal control signals, i.e. FT1, FT2, FT3, FT4, and V1, based on the selected operating mode, the operating conditions and the plant states; trying to maximize the distillate production and thermal efficiency of the MD module. It should be pointed out that the control problem changes in each of the operating modes since not all the variables are involved in all the operating modes. Also, in some of them, the MD module

is not in operation, so the objectives of the optimization problem also differ from the aforementioned ones. In what follows, the design of the two blocks is presented.

4.1. State machine

Three different operating modes have been differentiated for the SMD plant:

- **Mode 1:** This mode is used to heat the storage tank. The MD module cannot be operated under 60 ºC since it is not economically profitable (Gil et al., 2018a). So, if the tank is unloaded in terms of thermal energy, the solar field is used to heat the tank fast until reaching the required operating temperature by the MD module. The rules for selecting this operating mode are: TT1≤TT2, I≥I_{th}, and TT3≤T_{th}, where I_{th} and T_{th} are the threshold values of global irradiance and temperature in the tank required to turn on the solar field and MD module respectively, which are calculated as presented in (Gil et al., 2018a). In this operating mode, the control variables used by the NMPC controller are FT1 and V1, and the main objective is to increase the temperature in the upper part of the tank.

- **Mode 2:** In this mode, the solar field feeds the storage tank, which, in turn, is used to power the MD module. The rules used for selecting this mode are: TT1≤TT2, I≥I_{th}, and TT3≥T_{th}. In this case, the whole facility is in operation so that the control variables are FT1, FT2, FT3, FT4, and V1. However, different objectives can be differentiated for the optimal operation of the facility as increasing the temperature in the upper part of the tank and the one at the inlet of the heat exchanger, and increasing the distillate production and thermal efficiency of the MD module.

- **Mode 3:** This mode is used when the level of irradiance is low so that the solar field cannot be operated, but there is still enough thermal energy in the tank to operate the MD module. Here, the rules used are: TT1≥TT2, I≤I_{th}, and TT3≥T_{th}. In this mode, the control problem is simplified in comparison with the previous one being the control variables FT2, FT3, and FT4, and the objectives to increase the temperature at the inlet of the heat exchanger and to increase the distillate production and thermal efficiency of it.

Fig. 3 shows the flow that can occur among the different operating modes. Please note that, in the figure, mode 0 refers to an operating mode in which the SMD facility is turned off as none of the rules mentioned above are satisfied. Finally, it should be remarked that the rules are cheeked with mean values of the last ten minutes instead of using instantaneous ones thus avoiding chattering problems. Also, bumpless transfer mechanisms are used for switching among the different modes.

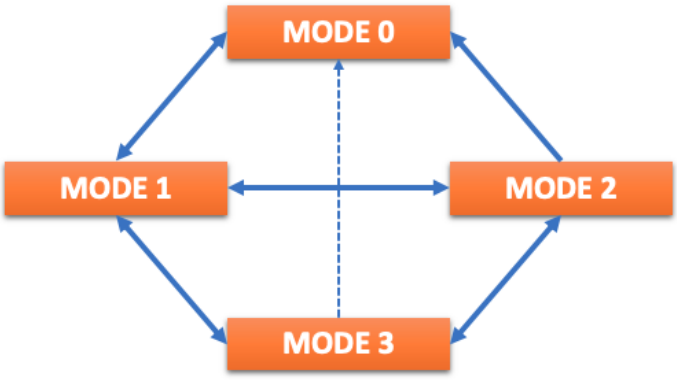

Fig. 3: Connections among operating modes.

4.2. NEPSAC controller

4.2.1. NEPSAC overview

Among the different MPC techniques, the NEPSAC (De Keyser, 2003) control strategy has been selected in this research work due to its favourable characteristics when dealing with nonlinear systems such as the whole model of the SMD plant used in this work. As other MPC strategies, the NEPSAC controller is based on the following three issues: i) the use of a model of the system at hand to predict the outputs along a determined prediction

horizon, ii) minimization of an objective function to calculate the future control signals, and iii) the use of a receding horizon strategy so that at each sampling time the first control signal is sent to the real system whereas the rest of the calculated sequence is rejected. The main difference among the different MPC techniques is the model used to represent the system and the disturbances. The NEPSAC algorithm is based on the Extended Prediction Self-Adaptive Control (EPSAC) technique proposed in (De Keyser, 2003), in which the model output $x(t)$ can be described as:

$$x(t) = f(x(t-1), x(t-2), \dots, u(t-1), u(t-2), \dots), \quad \text{(eq. 17)}$$

where $f(\cdot)$ can be a linear or a nonlinear function and $u(t)$ is the control input. Thus, the generic model used in this algorithm can be posed as:

$$y(t) = x(t) + n(t), \quad \text{(eq. 18)}$$

where $y(t)$ denotes the output of the system, $x(t)$ represents the model output and $n(t)$ is the model/process disturbance. In this work, $n(t)$ is calculated to remove the steady state error between the predictions and the real measured values:

$$n(t) = \frac{1}{1-q^{-1}} e(t), \quad \text{(eq. 19)}$$

being $e(t)$ the error and q^{-1} the backward shift operator.

Therefore, using the generic model in eq.18, the outputs along the prediction horizon can be computed as:

$$y(t+k|t) = x(t+k|t) + n(t+k|t), \quad \text{(eq. 20)}$$

for $k = N_1, \dots, N_2$ being N_1 and N_2 the minimum and maximum prediction horizons. Thus, the predictions of the process outputs are calculated using the measurements available at sampling time *t*, i.e., past outputs $[y(t), y(t-1), \dots]$ and past inputs $[u(t-1), u(t-2), \dots]$, and the value of the future control inputs $[u(t|t), u(t+1|t), \dots]$. Taking into account this last statement, eq. 20 can be rewritten as:

$$y(t+k|t) = y_{base}(t+k|t) + y_{opt}(t+k|t), \quad \text{(eq. 21)}$$

where $y_{base}(t+k|t)$ contains the effect of past inputs, the influence of a pre-specified future base control sequence $u_{base}(t+k|t)$, and the future predicted behaviour of disturbances $n(t+k|t)$. $y_{opt}(t+k|t)$ is related to the effect of the optimal control actions $\delta u(t|t), \dots, \delta u(t+N_u-1|t)$, where N_u is the control horizon and $\delta u(t+k|t) = u(t+k|t) - u_{base}(t+k|t)$. This optimized output can be computed as:

$$y_{opt}(t+k|t) = h_k \delta u(t|t) + h_{k-1}\delta u(t+1|t) + \cdots g_{k-N_u+1}\delta u(t+N_u-1|t), \quad \text{(eq. 22)}$$

where $h_1, \dots, h_{N_2}$ and $g_1, \dots, g_{N_2}$ are the unit impulse response and step response coefficients respectively. By expressing eq. 21 and eq. 22 on a matrix way, the MPC formulation emerges:

$$\mathbf{Y} = \bar{\mathbf{Y}} + \mathbf{GU}, \quad \text{(eq. 23)}$$

where:

$$\mathbf{Y} = [y(t+N_1|t), \dots, y(t+N_2|t)]^T, \quad \text{(eq. 24)}$$

$$\bar{\mathbf{Y}} = [y_{base}(t+N_1|t), \dots, y_{base}(t+N_2|t)]^T, \quad \text{(eq. 25)}$$

$$\mathbf{U} = [\delta u(t|t), \dots, \delta u(t+N_u-1|t)]^T, \quad \text{(eq. 26)}$$

$$\mathbf{G} = \begin{bmatrix} h_{N_1} & h_{N_1-1} & h_{N_1-2} & \dots & g_{N_1-N_u+1} \\ h_{N_1+1} & h_{N_1} & h_{N_1-1} & \dots & g_{N_1-N_u+2} \\ \dots & \dots & \dots & \dots & \dots \\ h_{N_2} & h_{N_2-1} & h_{N_2-2} & \dots & g_{N_2-N_u+1} \end{bmatrix}. \quad \text{(eq. 27)}$$

Once the model to calculate the predictions is obtained the control signals can be directly computed by minimizing a given objective function; as long as the function in eq. 17 be linear. It should be pointed out that, the calculation of the predictions in the form expressed in eq. 21 involves the use of the superposition principle, which does not hold in nonlinear systems. In this way, the strategy presented above is only valid from a practical

point of view when a nonlinear function in eq. 17 is used. Thus, by selecting an appropriate $\boldsymbol{u_{base}}$, the term $\boldsymbol{y_{opt}}$ in eq. 21 can gradually be zero in an iterative way. This then becomes the optimal solution as the superposition principle is no longer involved. This procedure is given by the following algorithm:

1. Initialize $u_{base}(t+1|t)$ at the optimal value computed in the previous sampling time.
2. Calculate matrix **G** using the nonlinear model in eq. 17 to obtain eq. 27. To do that, a unit impulse or step must be injected to the model in eq. 17 around the current operating trajectory.
3. Calculate $\delta u(t+k|t)$ for $k = 0 \dots N_u - 1$ by minimizing the given objective function and obtain the resulting control signals $u(t+k|t) = u_{base}(t+1|t) + \delta u(t+k|t)$ for $k = 0 \dots N_u - 1$.
4. Return to step 3 by taking the calculated $u(t+k|t)$ as the new set of $u_{base}(t+1|t)$.
5. Stop when $u_{base}(t+1|t)$ converges to the optimal value, which is that the difference between the value of $u_{base}(t+1|t)$ among two consecutive iterations is close to 0 or lower than a given tolerance.

4.2.2. NEPSAC applied to the SMD plant

The SMD plant can be classified as a Multiple Input Multiple Output (MIMO) system taking into account the different control variables, i.e., FT1, V1, FT2, FT3 and FT4, and the system outputs of interest to perform an optimal operation of the plant, i.e., TT3, TT9, D, and STEC. In this way, by following the NEPSAC technique described above, the predictions in this MIMO system can be calculated as:

$$\begin{bmatrix} \mathbf{Y_{TT3}} \\ \mathbf{Y_{TT9}} \\ \mathbf{Y_{D}} \\ \mathbf{Y_{STEC}} \end{bmatrix} = \begin{bmatrix} \mathbf{\bar{Y}_{TT3}} \\ \mathbf{\bar{Y}_{TT9}} \\ \mathbf{\bar{Y}_{D}} \\ \mathbf{\bar{Y}_{STEC}} \end{bmatrix} + \begin{bmatrix} \mathbf{G_{FT1}^{TT3}} & \mathbf{G_{V1}^{TT3}} & \mathbf{G_{FT2}^{TT3}} & \mathbf{G_{FT4}^{TT3}} \\ \mathbf{G_{FT1}^{TT9}} & \mathbf{G_{V1}^{TT9}} & \mathbf{G_{FT2}^{TT9}} & \mathbf{G_{FT4}^{TT9}} \\ \mathbf{G_{FT1}^{D}} & \mathbf{G_{V1}^{D}} & \mathbf{G_{FT2}^{D}} & \mathbf{G_{FT4}^{D}} \\ \mathbf{G_{FT1}^{STEC}} & \mathbf{G_{V1}^{STEC}} & \mathbf{G_{FT2}^{STEC}} & \mathbf{G_{FT4}^{STEC}} \end{bmatrix} \cdot \begin{bmatrix} \mathbf{U_{FT1}} \\ \mathbf{U_{V1}} \\ \mathbf{U_{FT2}} \\ \mathbf{U_{FT4}} \end{bmatrix}, \quad \text{(eq. 28)}$$

where vectors $\mathbf{Y_i}$, $\mathbf{\bar{Y}_i}$, $\mathbf{U_i}$ are arranged in the form presented in eqs. 24, 25 and 26 respectively, and matrix $\mathbf{G_i^j}$ in the way showed in eq. 27. Please note that FT3 has not been included in eq. 28 as it must be operated at the same level as FT4 in order to achieve maximum heat transfer in the heat exchanger (Gil et al., 2018a). It should also be pointed out that not all the control variables are physically related to all the system outputs. For example, the feed flow rate in the MD module (FT4) does not affect to the temperature in the storage tank (see Fig. 1). Thus, some of the terms can be removed from eq. 28 simplifying the calculations at each sampling time:

$$\begin{bmatrix} \mathbf{Y_{TT3}} \\ \mathbf{Y_{TT9}} \\ \mathbf{Y_{D}} \\ \mathbf{Y_{STEC}} \end{bmatrix} = \begin{bmatrix} \mathbf{\bar{Y}_{TT3}} \\ \mathbf{\bar{Y}_{TT9}} \\ \mathbf{\bar{Y}_{D}} \\ \mathbf{\bar{Y}_{STEC}} \end{bmatrix} + \begin{bmatrix} \mathbf{G_{FT1}^{TT3}} & \mathbf{G_{V1}^{TT3}} & \mathbf{0} & \mathbf{0} \\ \mathbf{0} & \mathbf{0} & \mathbf{G_{FT2}^{TT9}} & \mathbf{0} \\ \mathbf{0} & \mathbf{0} & \mathbf{0} & \mathbf{G_{FT4}^{D}} \\ \mathbf{0} & \mathbf{0} & \mathbf{0} & \mathbf{G_{FT4}^{STEC}} \end{bmatrix} \cdot \begin{bmatrix} \mathbf{U_{FT1}} \\ \mathbf{U_{V1}} \\ \mathbf{U_{FT2}} \\ \mathbf{U_{FT4}} \end{bmatrix}. \quad \text{(eq. 29)}$$

Moreover, although eq. 29 is the general expression used to model the whole SMD plant, this function is also adapted to each of the operating modes of the plant, according to the variables involved in them. For instance, in mode 1, only the prediction of the temperature in the upper part of the tank ($\mathbf{Y_{TT3}}$) must be considered, as the rest of the plant is turned off. In mode 2, the whole function in eq. 29 must be used as the entire plant is in operation. Finally, in mode 3, the prediction of the temperature in the upper part of the tank ($\mathbf{Y_{TT3}}$) can be removed as the solar field is turned off. Therefore, at each sampling time, the NEPSAC controller receives the selected operating mode by the state machine, as presented in Fig. 2, and computes only the necessary terms of the matrix, thus reducing the computing time requirements.

The last step in the NEPSAC technique is to formulate the objective functions used to calculate the optimal control actions in each of the operating modes. These functions can be posed according to the objectives described in section 4.1. Besides, due to the physical relationship among input and output variables (see eq. 29) and due to the arrangement of the real facility (see Fig. 1), we can decouple the whole optimization problem into two different ones: one to calculate the optimal control signals related to the solar field circuit (FT1, V1, FT2), and another one to calculate the control signal related to the MD module (FT4). In the first case, the objective is to maximize the temperature in the upper part of the tank and the temperature at the inlet of the heat exchanger, so the objective function can be formulated as:

$$J_1 = -\sum_{k=1}^{N_2} y_{TT3}(t+k|t) - \sum_{k=1}^{N_2} y_{TT9}(t+k|t). \quad \text{(eq. 30)}$$

This cost function is used in the three operating modes of the plant, but it is adapted to each of them. In mode 1, only the first term in the function is taken into account, in mode 2, both terms are considered, and in mode 3, only the second term is used. Secondly, for the MD module, the objective is to maximize its distillate production and thermal efficiency. As commented before, these two variables require contrary operating conditions in the feed flow rate (FT4) so the following multiobjective optimization problem can be cast:

$$\begin{bmatrix} J_2 \\ J_3 \end{bmatrix} = \begin{bmatrix} \sum_{k=1}^{N_2} y_{STEC}(t+k|t) \\ -\sum_{k=1}^{N_2} y_D(t+k|t) \end{bmatrix}. \quad \text{(eq. 31)}$$

It should be remarked that both optimization problems are subjected to some constraints related to the physical limits of actuators and the operating constraints:

$$\begin{aligned} &7.5 \text{ L/min} \leq \text{FT1} \leq 20 \text{ L/min}, \\ &0 \text{ \%} \leq \text{V1} \leq 100 \text{ \%}, \\ &15 \text{ L/min} \leq \text{FT1} \leq 22 \text{ L/min}, \\ &6.66 \text{ L/h} \leq \text{FT4} \leq 10 \text{ L/h}, \\ &\text{TT2} \leq 100 \text{ }^{\text{o}}\text{C}. \end{aligned} \quad \text{(eq. 32)}$$

5. Results and discussion

A wide variety of simulations using the nonlinear dynamical model presented in section 3 and real meteorological data from PSA were performed. The simulations were carried out using MATLAB 2019b software and its optimization toolbox. Specifically, the *fmincon* algorithm was used to solve the optimization problem in eq. 30 and the *paretosearch* algorithm to work out the one in eq. 31 (MATLAB, 2019). The sampling time of the control strategy was 5 min according to the system dynamics (Gil et al., 2018a). The prediction and control horizon were fixed at $N_1 = 1,\ N_2 = 10, N_u = 1$, which were chosen after exhaustive simulations until obtaining the desired closed loop response and following traditional recommendations in MPC techniques, i.e, $N_u \ll N_2$. In the following subsections the main results obtained are analyzed.

5.1. Multiobjective optimization problem: Pareto front.

Before analyzing the performance of the control algorithm during typical operating days, it is important to visualize the Pareto front obtained at each sampling time in the mutiobjective optimization problem in eq. 31, as well as to establish the selection of the optimal operating point. The Pareto front can be observed in Fig. 4.

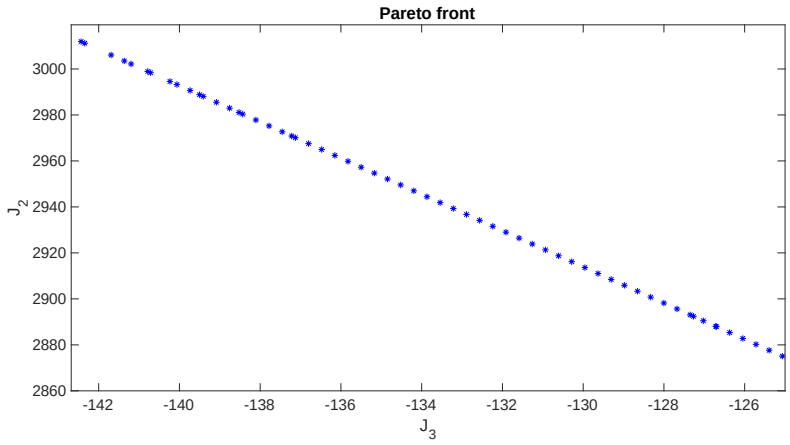

Fig. 4: Pareto front obtained in a single sampling time.

In this case, the Pareto front is composed of 60 points representing the different optimal points that can be adopted to maximize the thermal efficiency and the distillate production of the MD module. In this work, the middle point has been used as optimal solution, which represents the tradeoff solution among the two objectives. However, it should be commented that in real cases, the solution must be chosen according to the operating requirements, i.e., a given water demand.

5.2. Simulation results

In this subsection, the results obtained during a week operating the facility are presented. The simulation results are shown in Fig. 5. In this figure, the first graph (a) shows the irradiance conditions. Please note that the week chosen includes sunny and cloudy days thus increasing the reliability of the obtained results. The second graph (b) presents the temperatures of the SMD plant. The third one (c) includes the specific thermal consumption (STEC) and distillate production of the MD module. The fourth one (d) presents the control actions associated with each of the pumps of the SMD plant whereas the fifth one (e) shows the valve 1 aperture. The last one (f) includes the selected operating mode by the state machine.

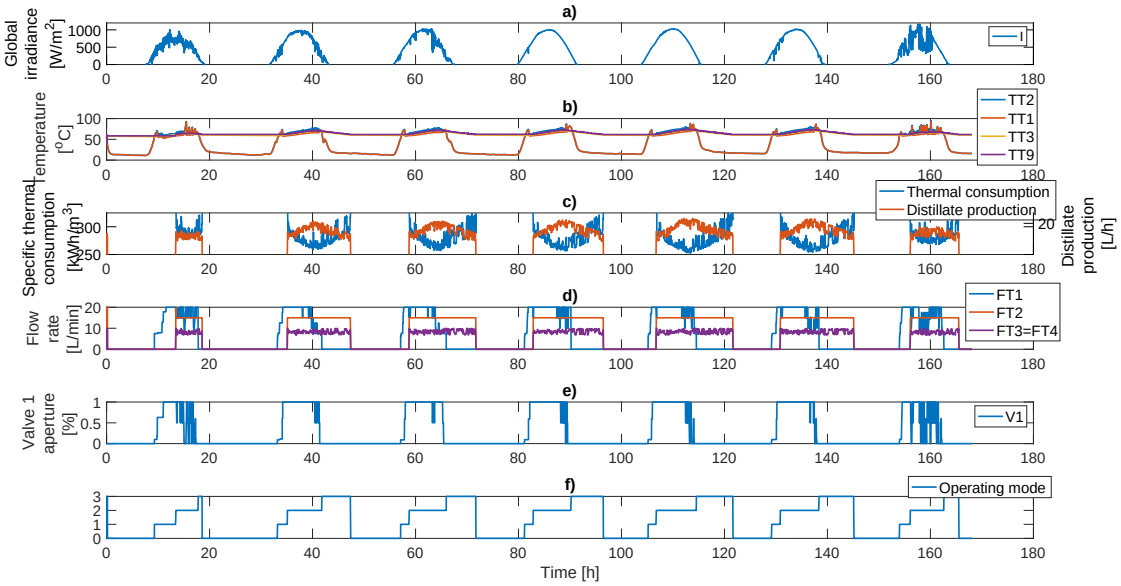

Fig. 5: Simulation results.

In general terms, it can be observed how in all the days the procedure is similar. The operation starts in mode 1 until reaching the required operating point in the storage tank to turn on the MD module. Then, the plant operates in mode 2 until the level of irradiance is low, preventing to load the storage tank. At this point, the state machine selects mode 3 and it maintains this operating mode until the tank is discharged in terms of thermal energy. It should be pointed out that the time during which the SMD plant operates in mode 3 depends on the irradiance conditions of each day. It can also be seen how the NEPSAC controller selects the optimal control actions in each of the operating modes according to the established objectives.

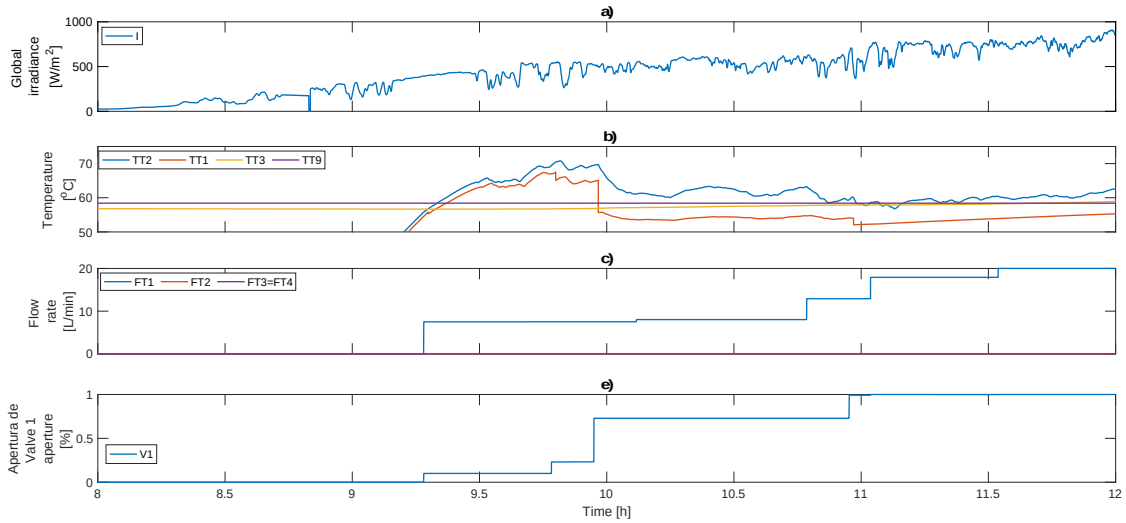

Fig. 6: Results of the first operating day when the state machine selects mode 1.

To highlight the performance of the NEPSAC controller, Fig. 6 presents the beginning of the first operating day when the state machine chooses the operating mode 1. Please remember that in this mode the objective is to heat

the tank fast, which is to increment the temperature at the top of the storage tank. In this way, it can be seen how the NEPSAC controller manages the valve 1 (V1) aperture and the solar field flow rate (FT1) to achieve this. Specifically, it gradually opens valve 1 towards the tank in a controlled way (see Fig. 6-d), pulling out cold fluid from the lower part of the tank, warming it by using the solar field, and inserting it by the upper part of the tank. Also, it regulates the flow rate (see Fig. 6-c) according to the operating conditions in terms of temperature (see Fig. 6-b) and global irradiance (see Fig. 6-a), preventing to load the tank with cold fluid (see Fig. 6-b).

5.3. Comparison with a manual operation

In order to demonstrate the good performance of the designed control strategy, the results presented in Fig. 5 were compared to those obtained in a manual operation. In the manual operation, the state machine was used with the same rules presented in section 4.1 but maintaining the actuators operating in a fixed point, which was selected following the ones usually used by the operators of the real facility at PSA.

Thus, three different metrics were selected to perform the comparison: i) the mean STEC of the whole simulation test, ii) the total distillate production, and iii) the number of operating hours of the MD module. The results showed how the thermal efficiency could be improved by 4 %, the total distillate production by 29 %, and the number of operating hours of the MD module by 16 %. Similar results can be found in different simulation scenarios.

6. Conclusions

This paper proposes an optimal operating strategy to improve the thermal efficiency and distillate production of a Solar Membrane Distillation plant in real-time. The operating strategy is based on a control structure composed of a state machine and an NMPC strategy based on the NEPSAC algorithm. The following conclusions can be drawn from the obtained results:

1. The proposed control technique has resulted in a powerful tool to optimally manage the SMD plant with different irradiance conditions.
2. The obtained metrics improved those of a manual operation. For example, the distillate production can be improved by up to 29 % whereas the specific thermal energy consumption by up to 4 %. These improvements could mean significant advanced towards the commercialization of the technology.

7. Acknowledgments

This work has been financed by the MICROPROD-SOLAR project of the Spanish State Research Agency (ref. PCI2019-103378), which supports the CYTED program call for Strategic Projects on distributed generation, renewable energies and microgrids in Strategic Enclaves of Latin America. Juan D. Gil acknowledges the financial assistance of the University of Almería through its Research and Transfer Plan.

8. References

Andrés-Mañas, J. A., Ruiz-Aguirre, A., Acién, F. G., Zaragoza, G., 2020. Performance increase of membrane distillation pilot scale modules operating in vacuum-enhanced air-gap configuration. Desalination, 475, 114202.

Bendevis, P., Karam, A., Laleg-Kirati, T. M., 2020. Optimal model-free control of solar thermal membrane distillation system. Computers & Chemical Engineering, 133, 106622.

Chang, H., Wang, G. B., Chen, Y. H., Li, C. C., Chang, C. L., 2010. Modeling and optimization of a solar driven membrane distillation desalination system. Renewable Energy, 35(12), 2714-2722.

De Keyser, R., 2003. Model Based Predictive Control. Invited Chapter in UNESCO Encyclopaedia of Life Support Systems Article contribution 6.43. 16.1.

Ghaffour, N., Lattemann, S., Missimer, T., Ng, K. C., Sinha, S., Amy, G., 2014. Renewable energy-driven innovative energy-efficient desalination technologies. Applied Energy, 136, 1155-1165.

Gil, J. D., Roca, L., Ruiz-Aguirre, A., Zaragoza, G., Berenguel, M., 2018a. Optimal operation of a solar membrane distillation pilot plant via nonlinear model predictive control. Computers & Chemical Engineering, 109, 151-165.

Gil, J. D., Ruiz-Aguirre, A., Roca, L., Zaragoza, G., Berenguel, M, 2018b. Prediction models to analyse the

performance of a commercial-scale membrane distillation unit for desalting brines from RO plants. Desalination, 445, 15-28.

Gil, J.D., Roca, L., Berenguel, M. 2020. Modelling and automatic control in solar membrane distillation: Fundamentals and proposals for its technological development. Revista Iberoamericana de Automática e Informática Industrial (In press). https://doi.org/10.4995/riai.2020.13122

Guillén-Burrieza, E., Blanco, J., Zaragoza, G., Alarcón, D. C., Palenzuela, P., Ibarra, M., Gernjak, W., 2011. Experimental analysis of an air gap membrane distillation solar desalination pilot system. Journal of Membrane Science, 379(1-2), 386-396.

Guillén-Burrieza, E., Alarcón-Padilla, D. C., Palenzuela, P., Zaragoza, G., 2015. Techno-economic assessment of a pilot-scale plant for solar desalination based on existing plate and frame MD technology. Desalination, 374, 70-80.

Guo, X., Albalawi, F., Laleg-Kirati, T. M., 2020. Observer-based economic model predictive control for direct contact membrane distillation. Chemical Engineering Research and Design, 156, 86-99.

MATLAB, 2019. MATLAB optimization toolbox release 2019b. Natick, MA, USA: The MathWorks.

Porrazzo, R., Cipollina, A., Galluzzo, M., Micale, G., 2013. A neural network-based optimizing control system for a seawater-desalination solar-powered membrane distillation unit. Computers & Chemical Engineering, 54, 79-96.

Thomas, N., Mavukkandy, M. O., Loutatidou, S., Arafat, H. A., 2017. Membrane distillation research & implementation: Lessons from the past five decades. Separation and Purification Technology, 189, 108-127.

Zaragoza, G., Ruiz-Aguirre, A., Guillén-Burrieza, E., 2014. Efficiency in the use of solar thermal energy of small membrane desalination systems for decentralized water production. Applied Energy, 130, 491-499.

WWAP, 2018. The United Nations World Water Development Report 2018: Nature-based Solutions for Water. Paris, UNESCO.

Appendix: Variables, Units and Symbols

Table 1: Variables of interest monitored in the SMD facility at PSA.

Description	Symbol	Unit
Distillate production	D	L/h
Solar field flow rate	FT1	L/min
Distribution system flow rate	FT2	L/min
Heat exchanger flow rate	FT3	L/min
Feed water flow rate	FT4	L/h
Global irradiance	I	W/m^2
Ambient temperature	T_a	ºC
Inlet solar field temperature	TT1	ºC
Outlet solar field temperature	TT2	ºC
Temperature at the top of the storage tank	TT3	ºC
Inlet distribution system temperature	TT4	ºC
Inlet heat exchanger temperature, hot side	TT5	ºC
Outlet heat exchanger temperature, hot side	TT6	ºC
Outlet distribution system temperature	TT7	ºC
Temperature at the bottom of the storage tank	TT8	ºC
Outlet heat exchanger temperature, cold side	TT9	ºC
Inlet heat exchanger temperature, cold side	TT10	ºC
Valve 1 aperture	V1	%

Table 2: Symbols and constants used in the model of the SMD plant.

Description	Symbol	Unit
Heat exchanger area	A_{he}	1.65 m^2
Cross-section area of one fluid inside the flat-plate collector	A_{sf}	1.539·10^{-4} m^2
Conversion factor to account for connections, number of modules and unit conversion	c_1	108 ·10^4 s L/(min m^3)
Conversion factor	c_2	6·10^4 s L/(min m^3)
Specific heat capacity of water	c_p	J/(kg ºC)
Specific heat capacity of sea water	$c_{p.sw}$	J/(kg ºC)
Solar field global thermal losses coefficient	H_1	5.88 J/(s ºC)
Tank thermal losses coefficient, upper part	H_2	3.6 J/(s ºC)
Tank thermal losses coefficient, lower part	H_3	3.8 J/(s ºC)
Collector absorber tube length	L_a	1.95 m
Equivalent absorber tube length	L_{eq}	m
Distribution system mass flow rate	$\dot{m}_{ds}$	kg/s
Equivalent solar field mass flow rate	$\dot{m}_{eq}$	kg/s
Heat exchanger mass flow rate	$\dot{m}_{he}$	kg/s
Membrane distillation module mass flow rate	$\dot{m}_{MD}$	kg/s
Solar field mass flow rate	$\dot{m}_{sf}$	kg/s
Number of series connections in a collector group	n_{cs}	5
Equivalent absorber tube mean temperature	$\bar{T}$	ºC
Volume, first stratification	V_1	0.75 m^3
Volume, second stratification	V_2	0.75 m^3
Heat exchanger heat transfer coefficient	α	670.80 W/(m^2 K)
Irradiance model parameter	β	0.11 m
Heat exchanger auxiliary factor 1	η_1	-
Heat exchanger auxiliary factor 2	η_2	-
Heat exchanger auxiliary factor 3	θ	-
Demineralized water density	ρ	kg/m^3

Table 3: Symbols and constants used in the formulation of the control system.

Description	Symbol	Unit
Error between the model output and the real system output	$e(\cdot)$	-
Step response coefficient	g	-
Matrix of unit impulse and step response coefficients	$\mathbf{G}$	-
Unit impulse response coefficient	h	-
Value of global irradiance necessary to turn on the solar field	I_{th}	W/m^2
Model/process disturbance	$n(\cdot)$	-
Minimum prediction horizon	N_1	-
Maximum prediction horizon	N_2	-
Control horizon	N_u	-
Backward shift operator	q^{-1}	-
Value of temperature necessary to turn on the MD module	T_{th}	ºC
Control input	$u(\cdot)$	-
Base control sequence	$u_{base}(\cdot)$	-
Vector of control actions	$\mathbf{U}$	-
Model output	$x(\cdot)$	-
Output of the system	$y(\cdot)$	-
Variable containing the effect of past inputs and outputs and predicted disturbances	$y_{base}(\cdot)$	-
Variable containing the effect of the optimized control actions	$y_{opt}(\cdot)$	-
Vector of system outputs	$\mathbf{Y}$	-
Vector of y_{base}	$\bar{\mathbf{Y}}$	-
Control action increment	δu	-